GEOPHYSICS, VOL. 55, NO. 10 (OCTOBER 1990); P. 1338–1346, 13 FIGS.

Spectral analysis in airborne electromagnetics

David C. Bartel* and Alex Becker‡

ABSTRACT

Interpretation of airborne electromagnetic (AEM) data is mainly concerned with determining the position, dip, depth, and quality (or conductance) of an anomalous geologic feature. A new method of interpretation using spectral analysis has certain advantages over conventional methods. It is specifically applied to the interpretation of AEM anomalies observed with the INPUT[1] time-domain electromagnetic system that are related to thin rectangular conductive plates. Profiles of field data are converted to the wavenumber domain by applying a Fourier transform. Because the amplitude spectrum varies exponentially with the distance from the target to the receiver, the target depth is easily interpreted from the slope of a semilogarithmic plot of the spectrum. Analytical expressions for the amplitude spectrum of an AEM anomaly can only be obtained for a rudimentary model where the target is represented by a single filament of induced current. The spectra of more realistic models such as the dipping infinitely conductive half-plane and the thin rectangular plate of finite conductance must be obtained numerically. The computed spectra are relatively insensitive to the target dip, except for the case of a horizontal target of finite width. For a flat-lying target, the spectrum exhibits a distinctive modulation pattern from which the target width can be determined. At low wavenumbers the time-decay characteristics of a given target are preserved so that its conductance can be determined. In most cases, however, this parameter as well as the target dip are just as easy to evaluate directly from the observed field data.

The results obtained with the spectral analysis method of interpretation applied to field examples agree well with the known geology. Interpretation of field data requires correction for the velocity of the aircraft and the time constant of the receiver equipment. In the wavenumber domain, however, these effects are easily eliminated by a simple division.

The spectral analysis method of electromagnetic interpretation is useful for determining the depth of the target because it is unaffected by dip, size, conductance, or profile position. One application of this method is in automated interpretation of portions of AEM data profiles, with large data sets over many conductors. Anomalies of interest can be picked out and interpreted automatically.

[1]Trademark of Barringer Research Ltd.

INTRODUCTION

Airborne electromagnetic (AEM) induction techniques are used extensively in the direct search for base metal deposits. Many surveys have resulted in discoveries because such deposits resemble an excellent confined electrical conductor surrounded by resistive host rock. The interpretation of the acquired data, however, may be problematic and conventional interpretation methods can lead to erroneous estimates of the target depth, dip, and quality. With the exception of one moderately successful attempt to use inversion theory (Keating, 1987), virtually all industrial practice relies on nomograms constructed from numerical or laboratory scale-model data. The classical method is described by Grant and West (1965, p. 554–555). Its successful use, as with any nomographic method, depends highly on the choice of the model data. Furthermore, as demonstrated by Bartel and Hohmann (1985), the target dip and depth estimates are interrelated, so that incorrect estimates of dip can result in substantial errors in the estimated depth. Given the large

Presented in part at the 57th and 58th Annual International Meetings, Society of Exploration Geophysicists. Manuscript received September 20, 1989; revised manuscript received March 16, 1990.
*Formerly Engineering Geoscience, University of California at Berkeley and Chevron Resources Company; presently Chevron USA, Inc., P.O. Box 5042, San Ramon, CA 94583-0942.
‡Engineering Geoscience, University of California at Berkeley, 414 Hearst Mining Building, Berkeley, CA 94720.

amount of AEM data routinely interpreted, one is led to ask whether it is possible to devise a rapid data interpretation technique that is not model-specific and yet yields good estimates of the target depth.

In many ways this problem resembles interpreting aeromagnetic data where classical nomographic methods have encountered difficulties similar to those described above for AEM data. In the case of magnetics, it has been shown that spectral analysis is useful for interpreting field results (Spector and Bhattacharyya, 1966; Spector and Grant, 1970). In this respect we note that the Fourier transform of the complicated expression describing the anomaly of a magnetized inclined dike is a simple negative exponential (Cassano and Rocca, 1975) whose decay rate is directly proportional to the target depth.

These observations, coupled with some mathematical similarities between the expressions for the magnetic anomaly of a dike and the approximate empirical description of an electromagnetic anomaly (e.g., Telford et al., 1976, p. 555–556, 564–565) brought us to examine the possibility of using spectral analysis to determine the depths of tabular conductors from the recorded AEM data. Because AEM anomalies do not generally admit a simple analytical formulation, our approach is of necessity numerical and hence, to some degree, empirical. We were, however, able to examine a large number of theoretical cases for the INPUT towed-bird configuration and can demonstrate that spectral analysis is indeed a valid technique for interpreting AEM data. Our conclusion is reinforced by testing this approach on a number of field examples (Bartel, 1988), two of which are included here.

FOURIER TRANSFORMS OF AEM ANOMALIES

We examine the utility of spectral analysis for AEM data interpretation by first considering the Fourier transforms for some elementary but crude approximations to AEM data which can be treated analytically. We then consider transforms for more realistic models which must be examined numerically. We employ the conventional definition of the Fourier transform given by

$$F(k_x) = \int_{-\infty}^{+\infty} f(x) e^{ixk_x}\, dx. \tag{1}$$

Here, the x coordinate is taken along the flight path assumed to be perpendicular to the strike of the target and lying directly over the center.

The secondary magnetic field as a function of x is thus transformed into a function of the angular wavenumber k_x. More common is the use of the ordinary wavenumber η_x which is related to k_x by a factor of 2π, [$\eta_x = k_x/2\pi$]. It has units of cycles per meter, or (what we will be using here) cycles per km. The time or frequency dependence of the data will not be considered because the general shape of an EM data profile is largely independent of those parameters. Because we are only concerned with the shape of the transform as a function of the wavenumber, the units of $F(k_x)$ (which are amperes for absolute values of the magnetic field or meters where relative values of this quantity are concerned) are of no interest here.

We consider only the INPUT system configuration because of its widespread use and consequent availability of field data. This system, recently described by Zollinger et al. (1987), is basically the same as the GEOTEM[2] system described by Thomson (1987). Of main interest to us is the coil configuration shown in Figure 1. It consists of a vertical axis transmitter loop attached to the aircraft which flies at a nominal altitude of 120 m. The receiver is a small solenoid whose axis is horizontal, towed behind the aircraft in a bird whose position depends on many factors including air speed (Annan, 1983). In its normal position, however, the receiver is located about 96 m behind and 67 m below the aircraft.

THE LINE CURRENT TARGET

As suggested by Keller and Frischknecht (1966), the simplest approximation to the eddy current distribution in a tabular conductor is a long filament of current of strength I that coincides with its upper edge. The filament lies along the y-axis and the measurements are taken along the x-axis at a height z above the filament. In this case, the magnetic field is given by

$$H_x(x, z) = \frac{I}{2\pi} \frac{z}{x^2 + z^2}, \tag{2}$$

and

$$H_z(x, z) = \frac{I}{2\pi} \frac{x}{x^2 + z^2}. \tag{3}$$

The Fourier transform of these two equations can be found using Erdelyi et al. (1954, no. 3.1.10 and 3.2.5) to yield

$$\hat{H}_x(k_x, z) = \frac{I}{2\pi} e^{-z|k_x|}, \tag{4}$$

[2]Trademark of Geoterrex, Ltd.

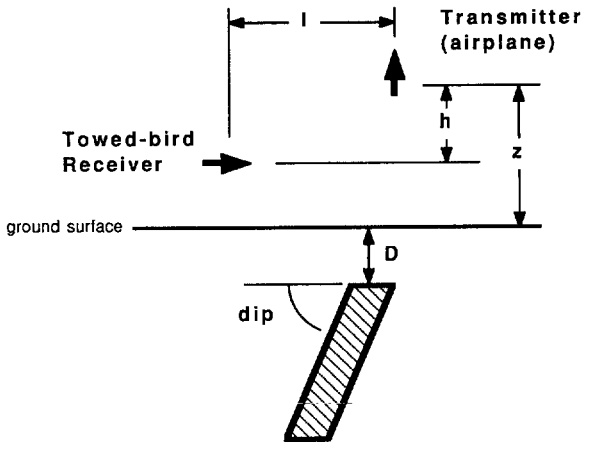

FIG. 1. INPUT system configuration; ℓ is the horizontal transmitter-receiver separation; h is the vertical transmitter-receiver separation, z is the altitude of the airplane, and D is the target depth.

and

$$\hat{H}_z(k_x, z) = \frac{-iI}{2\pi} e^{-z|k_x|} \tag{5}$$

which are valid for positive k_x only. $H_x(k_x, z)$ and $H_z(k_x, z)$ differ only in phase; their amplitude spectra are identical. For this simple approximation, the depth of the line source can be determined directly from the slope of the amplitude falloff in the wavenumber domain when the spectrum is plotted on semilogarithmic paper.

A higher degree of reality can be introduced by considering the coupling between the AEM system and a current filament. Following Telford et al. (1976, p. 511, 514–519, 555–556), the inductive limit normalized secondary magnetic field at the receiver can be written as

$$h_{zx} = \frac{H^S_{zx}}{H^P_{zx}} = C \frac{x + \ell/2}{(x + \ell/2)^2 + z^2} \frac{z - h}{(x + \ell/2)^2 + (z - h)^2}, \tag{6}$$

with

$$C = \frac{\mu}{\pi L} \frac{(h^2 + \ell^2)^{5/2}}{3\, h\ell};$$

where

H^P_{zx} = x-oriented primary magnetic field at the receiver due to a vertical dipole source,

H^S_{zx} = x-oriented secondary magnetic field at the receiver,

ℓ = lateral separation between transmitter and receiver,

h = vertical separation between transmitter and receiver, and

L = target inductance.

The origin for the coordinate system is taken at the midpoint between the receiver and transmitter. The Fourier transform of equation (6) can be carried out using the convolution theorem (Gradshteyn and Ryzhik, 1980) and standard forms (Erdelyi et al., 1954). The result is given by

$$\hat{h}_{zx}(k_x) = -iC\left[\frac{e^{-(z-h+i\ell/2)k_x}}{2z - h - i\ell} + \frac{e^{-(z-h-i\ell/2)k_x}}{h - i\ell} + \frac{e^{-(z-h+i\ell/2)k_x}}{2z - h + i\ell}\right]. \tag{7}$$

The complexity of the above function does not readily reveal that here too we basically have an exponential falloff of spectral amplitude with k_x. Equation (7) can be rearranged to better demonstrate the amplitude variation to be

$$\hat{h}_{zx}(k_x) = -iC' e^{i\ell k_x/2}[e^{-(z-h+i\ell)k_x}(a + ib) + e^{-zk_x}(c + id)], \tag{8}$$

where a, b, c, d, and C' are parameters that depend only on z, h, ℓ, and target conductance and size. Since $z - h < z$ for a towed-bird receiver system (such as INPUT or GEOTEM), the predominant decay will be dependent on

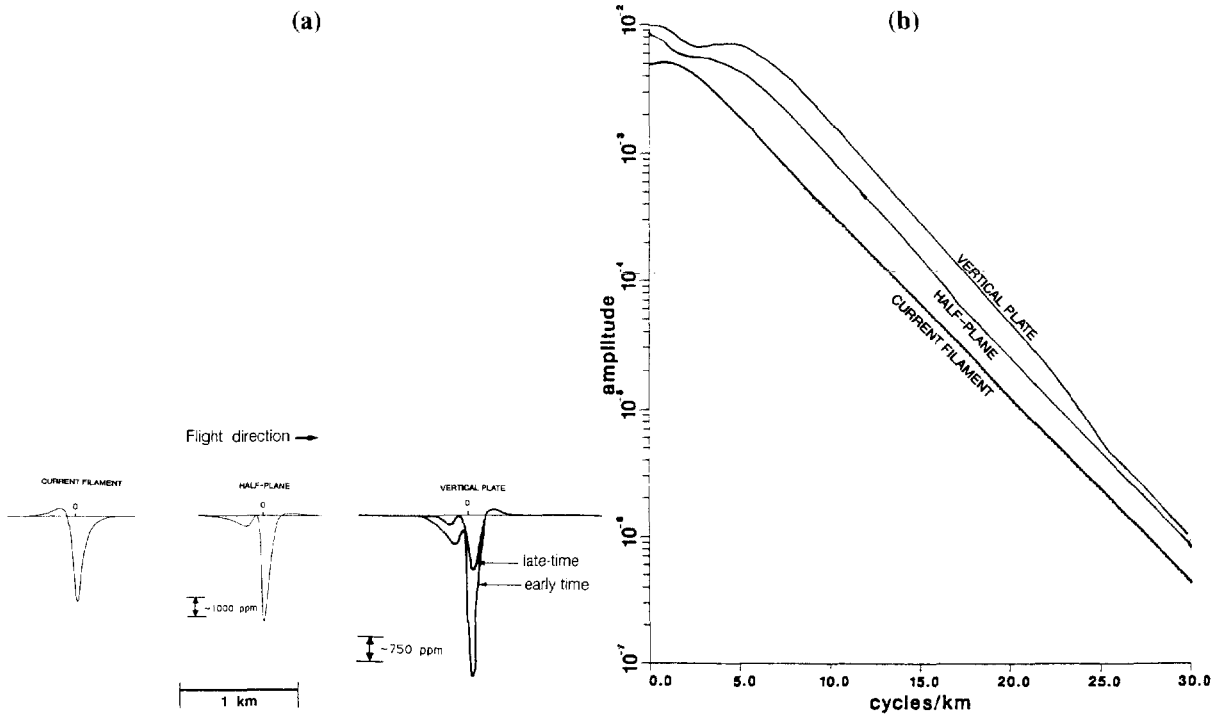

FIG. 2. Space-domain profiles and wavenumber-domain amplitude spectra for a vertical conductor model using the fixed-wing INPUT system for the current filament, half-plane, and thin finite plate approximations; (a) space-domain profiles; (b) wavenumber-domain amplitude spectra. All models are located 53 m below the receiver. Target centered at 0 on all profiles.

$z-h$ or the depth of the source below the receiver. This will be particularly true at higher wavenumbers.

A portion of Figure 2 is devoted to a graphical presentation of equations (6) and (7). The normalized magnetic field anomaly for the filament model is shown in the left part of Figure 2a, while the corresponding transform is shown in Figure 2b. In spite of the analytical complexity of equation (7), the power spectrum is clearly linear for wavenumbers in excess of 8 cycles/km. The slope of this portion of the spectral response yields the correct target-receiver distance of 53 m.

TABULAR MODELS

The next model we examine is the vertical half-plane. Analytical expressions for its inductive limit response are given by Wesley (1958). The corresponding spectral response can be readily computed using a standard FFT algorithm (Claerbout, 1985, p. 12). The results for this computation are also shown in Figure 2. Again we note the exponential decay of the amplitude spectrum and observe that the exponent is indeed approximately equal to the height of the receiver above the upper edge of the half-plane (53 m). To show that this unique relationship between the slope of the amplitude spectrum and the depth to the top edge of the target also holds outside the inductive limit and is valid for finite conductors, we examine the transform for a square vertical 300 × 300 m plate conductor. For this conductor, whose conductance is 100 S, we computed the response at 1 ms after cessation of a 1.8 ms half-sine pulse (i.e., INPUT transmitter pulse) using the University of Toronto program PLATE (Dyck et al., 1980). These results (labeled EARLY TIME) are also presented in Figure 2 to compare them with the other models. The exponential decay of the spectrum is again apparent between 9 and 22 cycles/km. Below a relative amplitude level of 10^{-5}, numerical inaccuracies in the original program PLATE computations and those arising from an FFT make amplitude spectra decay of the PLATE model nonexponential. In this case, however, its slope indicates a depth of 3 m below the top edge of the target, which is interpreted as a migration of the equivalent current filament toward the center of the target with time, as has been noted previously (Dyck, 1981; Barnett, 1984).

Returning to the inductive limit response of the half-plane model, we examine the effects of depth and dip. The effects of increasing depth to the top of the half-plane are a broadening and dampening of the observed anomalous response. In the wavenumber domain this manifests itself as an increase in the high-wavenumber slope and a general decrease in the magnitude of the amplitude spectrum. These changes in slope and amplitude are demonstrated in Figure 3 for the fixed-wing INPUT system. The depths noted for each curve refer to the depth below ground surface. The depths that may be calculated from the slope refer to the total depth below the receiver, including the receiver height above the imaginary ground surface, and accurately reflect the model depth used to compute the synthetic anomalies.

The effect of dip on the INPUT system anomalies is interesting. The entire range of dip from 0 degrees to 180 degrees needs to be studied because the INPUT configuration is asymmetrical. A series of simulated field data profiles for different dips of a half-plane is shown in Figure 4. Note that at shallow dips (~30 degrees), the largest peak response does not occur over the top of the half-plane. Turning to the spectral response, we observe that for a vertical half-plane as shown in Figure 2, there is a small flat spot apparent at low wavenumbers. As shown in Figure 5, this flat spot turns into a notch in the amplitude spectrum when the system is going updip (0 degree dips to 90 degrees). For dips greater than 90 degrees or with the system traveling downdip, the flat spot disappears and the amplitude decays somewhat uniformly from its zero-frequency value. In all cases, at higher wavenumbers the slope is exponential and the depth

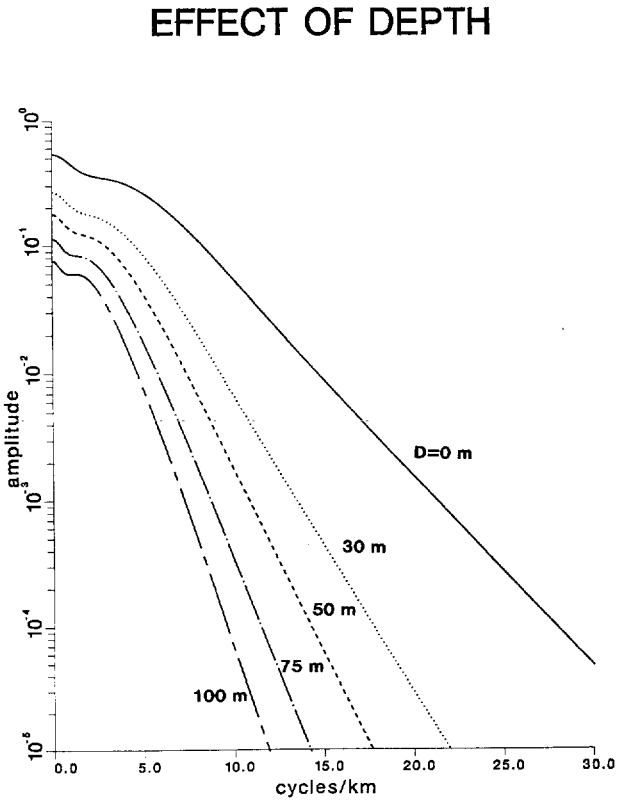

FIG. 3. Effect of depth on the amplitude spectrum of a vertical half-plane for the fixed-wing INPUT system; z = 120 m, h = 67 m, ℓ = 96 m, D = depth below ground surface (which is 53 m below the receiver).

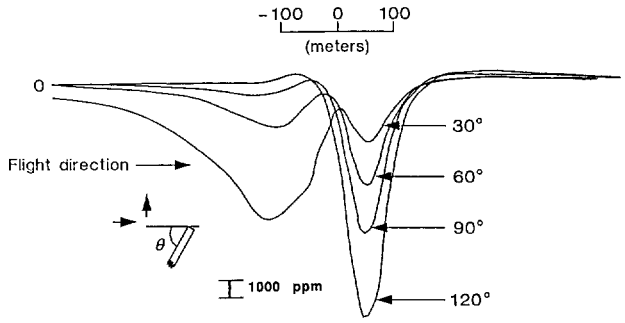

FIG. 4. Anomaly response changes with dip for the fixed-wing INPUT system.

may be determined from the slope. The amplitude spectra for all models where the dip was greater than 90 degrees were essentially the same. For finite-sized plates, the amplitude spectra are quite similar to those shown in Figure 5 (Bartel, 1988).

An interesting feature is observed for horizontal targets. For example, consider the anomalous response of a flat, thin target in the form of a 300 m square plate with a conductance of 100 S shown in Figure 6. The transform of the response shown in Figure 7 exhibits a nearly exponential envelope which is now modulated by a series of peaks and troughs. The amplitude spectra can be approximated by an exponential function of the form given in equation (8) multiplied by a sine term with an argument of $\pi W\eta_x$, where W is the target width. The spacing of the troughs is related to the width of the target. In particular, the width of the target is approximately $W = n/\eta_x$, where $n = 1, 2, 3, \ldots$ for each successive zero of the amplitude spectrum (Bartel, 1988). Note that at the later times, the troughs migrate to a higher wavenumber (i.e., smaller interpreted width) corresponding to a migration of the equivalent current filament to the center. Thus at 0.1 ms the interpreted width is approximately 345 m, at 1 ms it is 290 m, and at 10 ms it is approximately 165 m.

Not much mention has been made here concerning the phase spectrum. Numerically evaluating equation (7) demonstrates that it has a dominant linear variation with η_x related to the horizontal and vertical separations of the transmitter and receiver (Bartel, 1988). After removing the linear component, the phase spectrum can be useful in a qualitative evaluation of the dip of a target.

The space-domain to wavenumber-domain transformation does not affect the temporal variation of the target response. Thus the target time constant can be evaluated in either domain. It may be argued that estimation of the time decay in the wavenumber-domain is advantageous because there is no need to worry about migration of the peak response with time as can occur in the space domain (Dyck et al., 1975). Calculation of the target time constant is best made at low wavenumbers (e.g., 1 cycle/km) because here the amplitude

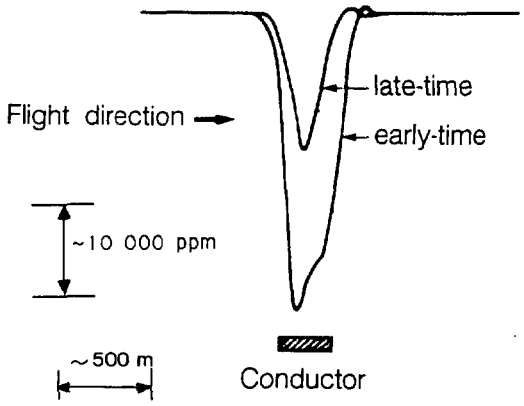

FIG. 6. Representative early- and late-time responses of a horizontal thin-plate target for the fixed-wing INPUT system (from Bartel and Becker, 1987).

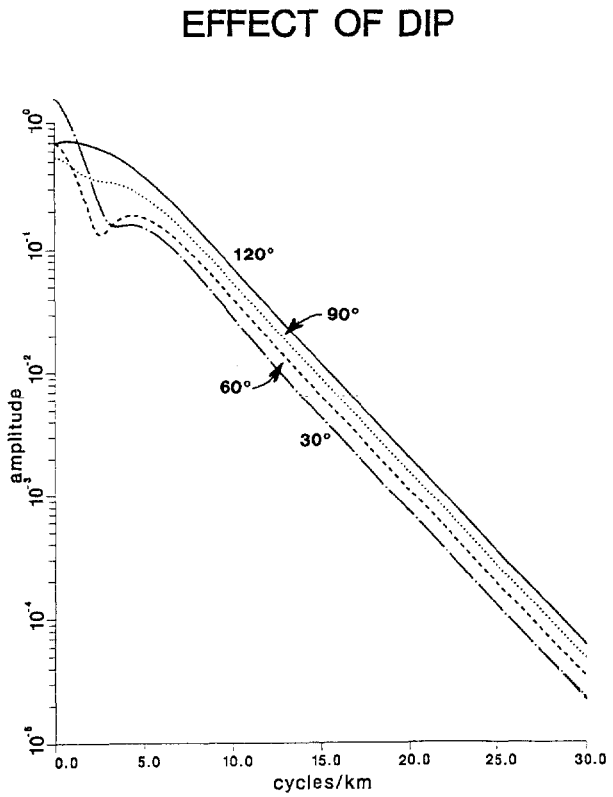

FIG. 5. Effect of dip on the amplitude spectrum for the fixed-wing INPUT system; z = 120 m, h = 67 m, ℓ = 96 m, D = 0 m. Refer to the space-domain profiles in Figure 4.

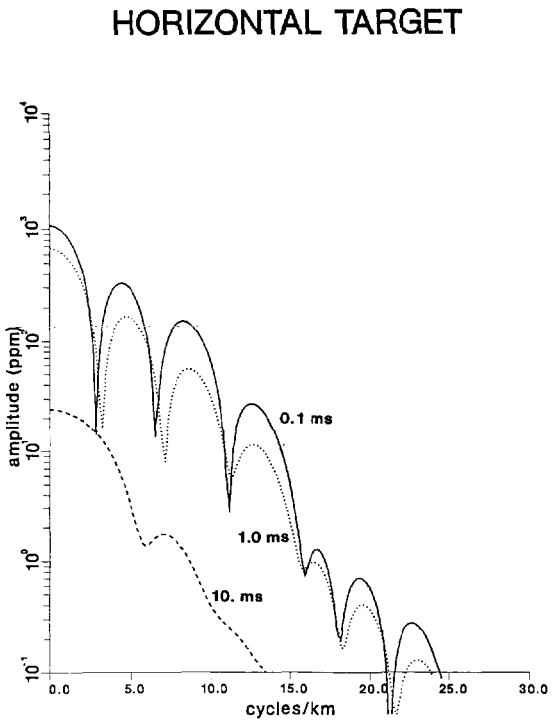

FIG. 7. Amplitude spectrum of a horizontal thin-plate target for the fixed-wing INPUT system; z = 120 m, h = 67 m, ℓ = 96 m. Target size is 300 m by 300 m; conductance is 100 S.

spectrum is most representative of the principal mode of current flow in the target. Estimation of the target time constant at dc ($\eta_x = 0$ cycles/km) is not suggested because of a possible amplitude shift or offset in the space-domain profile.

ANALYSIS OF FIELD DATA

No new interpretation method can be considered useful unless it is validated with field examples where the target parameters are known from drilling or excavation. One of the additional factors that must be considered in analyzing field data is that while measurements of the secondary field on the ground are static, an airborne system represents a dynamic system where the effects due to velocity of the airplane and the time constant of the receiver making the measurements must be taken into account. Both these effects can be incorporated into what will be called the "velocity correction."

Field data also contain a certain amount of noise, which can be due to minor variations in the geology, natural or manmade EM sources, changes in the separation of the transmitter and receiver, instrumentation, and possibly digitization of field curves. If the total amount of noise in the space-domain response is expressed as a percentage of the peak anomaly response, then Bartel (1988) showed that a noise level of <1 percent is necessary to allow for a reasonable range in the wavenumber domain to measure the amplitude spectrum decay. Higher noise levels limit the amount of amplitude range available for describing the spectrum by creating a noise "floor," In a gross sense this is reasonable because a spike or delta function in the space domain transforms to a constant in the wavenumber domain [Gabel and Roberts, 1980, equation (5.123)]. Two or three orders of magnitude in vertical resolution are sufficient for defining the amplitude spectrum.

Velocity correction

Dyck et al. (1975), Annan (1983), Becker and Cheng (1987), and Keating (1987) all recognized that airborne EM measurements are not made at discrete points but are influenced by the velocity of the aircraft and the time constant of the equipment. The receiver time constant determines the amount of signal stacking that occurs during the measurements. As explained by Becker and Cheng (1987), the observed system response is a convolution of the static target response with the impulse response of the equipment. In many cases the latter can be approximately represented by a single exponential term which includes the transit time of the airborne system along the profile and the equipment time constant. The transit time can be expressed as a function of the aircraft's velocity and position along the profile. Thus

$$F^*(x) = F(x) * \frac{1}{v\tau_e} e^{-x/v\tau_e} u(x/v), \tag{9}$$

where $F^*(x)$ is the observed response, $F(x)$ is the sampled static response measured at discrete points, v is the transit time, x is the position of the aircraft along the profile line, and τ_e is the time constant of the equipment. The convolution expressed in equation (9) becomes a multiplication operation after a Fourier transform converts the data from the space domain to the wavenumber domain due to the properties of the Fourier transform (Gradshteyn and Ryzhik, 1980, no. 17.22.3). Thus, equation (9) transforms to [using Gabel and Roberts, 1980, equation (5.90)]

$$F^*(k_x) = \frac{F(k_x)}{1 + iv\tau_e k_x}. \tag{10}$$

Based on equation (10), the amplitude spectrum of the field data needs to be modified to interpret it correctly in the same manner as the numerical models. The correction is

$$|F(k_x)| = |F^*(k_x)|[1 + (v\tau_e k_x)^2]^{1/2}. \tag{11}$$

The phase spectrum can be similarly corrected (Bartel, 1988).

Thierry deposit

The first field example is the Thierry copper-nickel massive sulfide deposit in the Pickle Lake region of northern Ontario. A geologic description along with the geophysical data for the INPUT and other geophysical systems is given by Caven (1976). A profile of the INPUT response flown from south to north over the deposit is given in Figure 8. A clear response can be seen in all six channels. The data from the published INPUT profile were digitized and processed in the manner described above.

First we demonstrate the effect of using the velocity correction in equation (11) on the amplitude spectrum of the target response. Since, for example, the actual speed of the aircraft and value of the receiver time constant are unknown, typical values for the fixed-wing INPUT system were used,

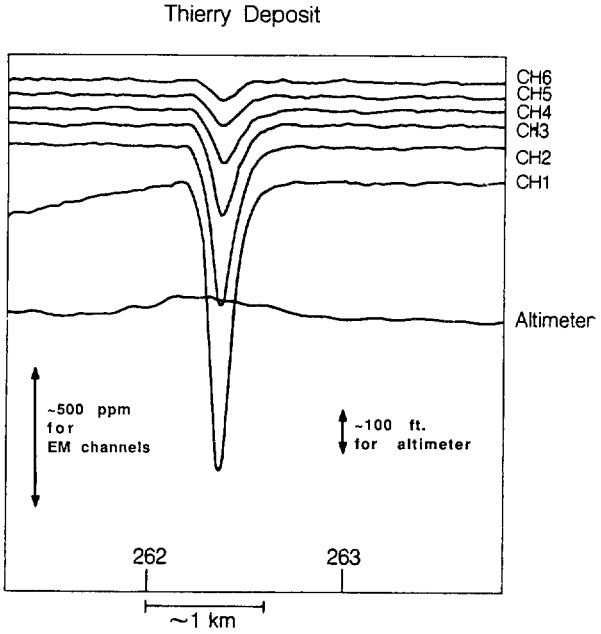

FIG. 8. Fixed-wing INPUT response for the Thierry deposit, Ontario (from Caven, 1976). Channels 1–6 are shown from bottom to top.

resulting in a $v\tau_e$ product of 100 m. The effect of the velocity correction on the channel 1 data is shown in Figure 9. The top curve is the corrected amplitude spectrum, while the uncorrected one is shown by the lower (solid) curve. The velocity correction decreases the high-wavenumber slope but does not affect the magnitude of the spectrum at $\eta_x = 0$ cycle/km. The reduced value of slope yields the correct depth value of 0 m below the surface; however, it does not increase the range over which to average the amplitude decay for an interpretation because the noise floor remains the same.

Correcting all channels of data for the aircraft velocity and equipment time constant showed that useful depth information can be obtained from the first four channels. The amplitude spectra of the channel 5 and 6 data decayed too quickly into the noise to be useful. Figure 10 shows the corrected amplitude spectra for the Thierry deposit. About two orders of magnitude of vertical resolution in the amplitude spectra were possible before noise due to the digitizing method and inherent in the field results becomes dominant. The depth can be interpreted from the slope between $\eta_x = 3$ and 6 cycles/km for each channel. On channel 1, this range could be extended out to $\eta_x = 8$ cycles/km but would yield the same depth information. The interpreted depth for the current axis is at the surface for channel 1 and about 75 m below the surface for channel 4. It is difficult to ascertain the dip angle from the amplitude spectra, but the low-wavenumber shape suggests a dip to the north. This agrees with the geologic information known by drilling and mining displayed in Figure 11, with the equivalent current axes for channels 1 and 4 also displayed.

Detour deposit

Reed (1981) described the discovery of the Detour zinc-copper-silver sulfide deposit in the Brouillan Township in northwestern Quebec with the fixed-wing INPUT AEM system. Along with the original INPUT profiles, Reed (1981) showed some forward modeling results to fit the response for the Detour deposit. Figure 12 shows one of the profiles that can be interpreted using the spectral analysis method.

Because of the high level of processing noise in the data, only the first three channels of data can be used effectively. The amplitude spectra after velocity correction are shown in Figure 13. The region from $\eta_x = 2.5$ to 5 cycles/km can be used to interpret the depth of the target. For the transmitter altitude and system geometry given in Reed (1981), the least-squares fit slope through this region indicates a depth to the current axis of 20 m below the surface. This result is in good agreement with the data reported by Reed (1981), which indicated a depth of 10–20 m.

DISCUSSION

The main product of the spectral analysis method of EM data interpretation is a simple estimate for the depth to the equivalent current axis in the target. This estimate is derived from the nearly exponential wavenumber-domain amplitude spectrum of a data profile. The rate of decay of this exponential is proportional to the vertical distance from the equivalent current axis in the target to the receiver above it. In most cases, the altitude of the receiver is sufficiently stable in any single profile, or at least the portion over the

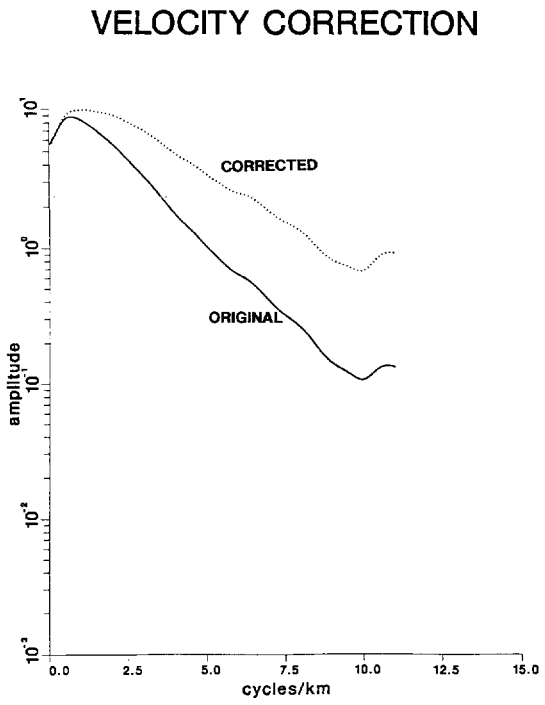

FIG. 9. Effect of velocity correction [equation (12)] on the amplitude spectrum for the channel 1 data over the Thierry deposit, Ontario; $v\tau_e = 100$ m.

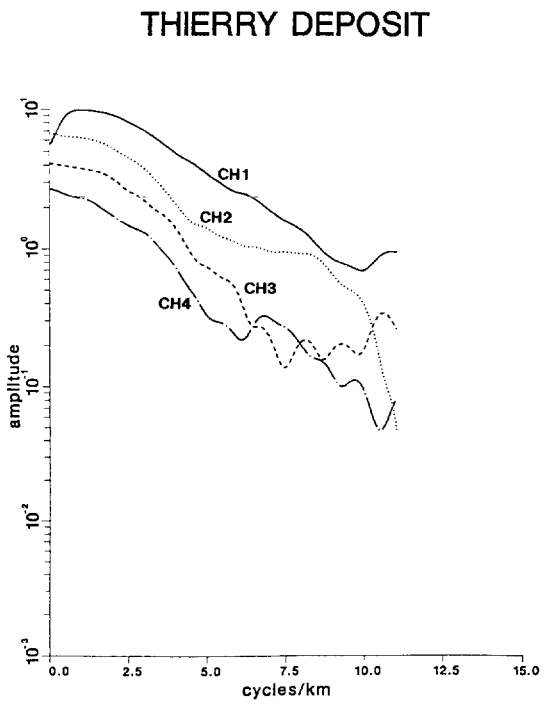

FIG. 10. Corrected amplitude spectra for the first four channels of the INPUT response over the Thierry deposit; correction done according to equation (11) with $v\tau_e = 100$ m.

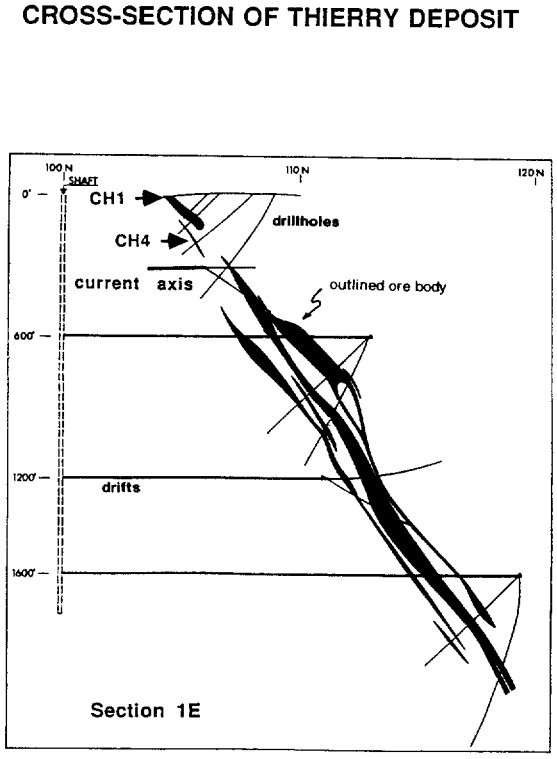

FIG. 11. Cross-section of the Thierry deposit with shaft, drifts, outlined orebody, and equivalent current axes for channels 1 and 4; cross-section from Caven (1976).

target, to be considered a constant. Thus the subsurface target depth can be estimated properly.

Spectral analysis may be used to interpret electromagnetic profiles over isolated conductors. The interpretation of the depth for a conductive body is quite simple and is relatively unaffected by target dip or the position of the data profile. The direction of the profile line relative to the strike of the body has only a minor influence on the interpreted depth (Bartel, 1988). The conductance and size of the thin-plate target affect the depth interpretation only to the extent that these parameters influence the target time constant. At later measurement times, the interpreted depth will be greater than at early times because the induced eddy currents collapse toward the center of the target. For horizontal conductors, the conductance and size of the target do not affect the interpreted depth but will affect the interpreted width of the target along the profile line. The interpretation of width can be made from the modulation of the amplitude spectrum. At this point we have insufficient experience with multiple conductors and targets covered by conductive overburden to use the spectral method of interpretation adequately in these cases.

In airborne surveying, the speed of the airplane or helicopter and the time constant of the receiver equipment cause a modification of the anomaly shape and magnitude. A correction for these elements is essential in interpreting field examples and is most easily performed in the wavenumber-domain where it involves only a simple multiplication with the static wavenumber domain response. Without this correction, any interpreted depth will be much greater than the

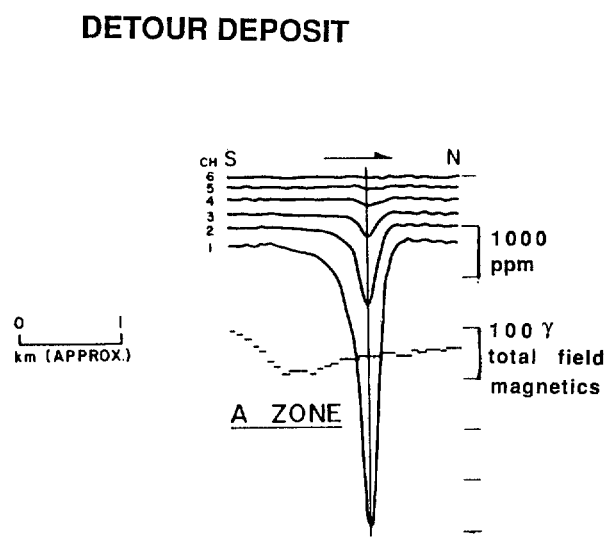

FIG. 12. Fixed-wing INPUT response over the Detour deposit, Quebec (from Reed, 1981). Channels 1–6 are shown from bottom to top.

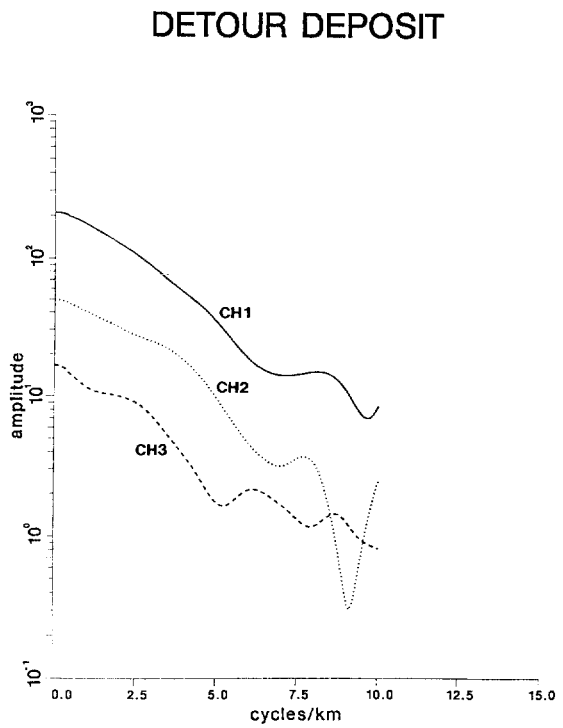

FIG. 13. Corrected amplitude spectra for the first three channels of the fixed-wing INPUT response over the Detour deposit; correction done according to equation (11) with $v\tau_e$ = 100 m.

true depth. Field data are also affected by noise which can be geologic or can be related to the instability of the system geometry. The effect of noise is to limit the vertical range available for measuring the amplitude spectrum decay.

A study of this nature always invites more questions than it can possibly answer, but there are certain avenues of investigation which could be pursued in order for this interpretation method to be more universally applied. The first would be a thorough testing of the wavenumber-domain response over a spherical conductor. As shown in Bartel (1988), the interpreted depth is certainly interior to the sphere, but cannot be simply related to its size or depth. The main differences between the interpretation for a prismatic or tabular target and for a spherical target are that in the latter case induced currents are not confined to flow in a single plane and their location in the conductor is dependent on the spatial relation between the transmitter and the target.

Use of the spectral analysis method for ground EM interpretation has not been addressed directly. If the transmitter and receiver are at the same level [i.e., $h = 0$ in equation (6)] as is generally true for a ground EM system, then the amplitude spectrum would need to be modified for the effect of the transmitter-receiver separation for the amplitude decay to closely resemble an exponential decay (see Bartel, 1988). The amplitude spectrum for central in-loop profiles would also not decay exponentially, but instead should approximate $k_x e^{-zk_x}$ as outlined in Bartel [1988, equations (2.54), (2.60), and (2.65)]. Interpretation for large fixed-loop or TURAM-type surveys should be simpler because the transmitter position is constant for each profile line. Hence, its height and position will be unimportant except in energizing the target and the wavenumber-domain response for a vertical target should resemble equation (4) or (5) depending on the receiver component. This type of survey configuration would also facilitate 2-D spectral analysis interpretation techniques as mentioned in Bartel (1988) if several profile lines of data for one transmitter location were obtained.

ACKNOWLEDGMENTS

Financial support for this research was provided in part by the Selco Division, BP Canada. Computer support was provided by the Earth Science Division, Lawrence Berkeley Laboratory, University of California. One author (DCB) would also like to thank Chevron Resources Company and Chevron USA, Inc. for permission to finish publishing this paper. We are also grateful for the helpful suggestions of the reviewers.

REFERENCES

Annan, A. P., 1983, Effect of differential transmitter/receiver motion on airborne transient EM interpretation: Presented at the 53rd Ann. Internat. Mtg., Soc. of Explor. Geophys., Las Vegas, NV.

Barnett, C. T., 1984, Simple inversion of time-domain electromagnetic data: Geophysics, **49,** 925–933.

Bartel, D. C., 1988, Spectral analysis in airborne electromagnetics: Ph.D. thesis, Univ. of California at Berkeley.

Bartel, D. C., and Becker, A., 1987, Spectral analysis in airborne electromagnetics: Presented at the 57th Ann. Internat. Mtg., Soc. of Explor. Geophys., New Orleans, LA.

Bartel, D. C., and Hohmann, G. W., 1985, Interpretation of Crone pulse electromagnetic data: Geophysics, **50,** 1488–1499.

Becker, A., and Cheng, G., 1987, Detection of repetitive electromagnetic signals, *in* Nabighian, M.N., Ed., Electromagnetic methods in applied geophysics, **1:** Soc. of Explor. Geophys., 443–468.

Cassano, E., and Rocca, F., 1975, Interpretation of magnetic anomalies using spectral estimation techniques: Geophys. Prosp., **23,** 663–681.

Caven, R. J., 1976, Geophysical surveying at the Umex Thierry deposit: Can. Min. J., **97,** no. 10, 34–43.

Claerbout, J. F., 1985, Fundamentals of geophysical data processing: Blackwell Scientific Publ.

Dyck, A. V., 1981, A method for quantitative interpretation of wideband, drill-hole EM surveys in mineral exploration: Res. in Appl. Geophys., **23,** Univ. of Toronto.

Dyck, A. V., Becker, A., and Colett, L. S., 1975, INPUT AEM results from Project Pioneer, Manitoba: Can. J. Earth Sci., **12,** 971—981.

Dyck, A. V., Bloore, M., and Vallee, M. A., 1980, User manual for programs PLATE and SPHERE: Res. in Appl. Geophys., **14,** Univ. of Toronto.

Erdelyi, A., Magnus, M., Oberhettinger, F., and Tricomi, F. G., 1954, Tables of integral transforms, **1:** McGraw-Hill Book Co.

Gabel, R. A., and Roberts, R. A., 1980, Signals and linear systems, 2nd Ed.: John Wiley and Sons.

Gradshteyn, I. S., and Ryzhik, I. M., 1980, Tables of integrals, series, and products, corr. and enlarged ed.: Academic Press.

Grant, F. S., and West, G. F., 1965, Interpretation theory in applied geophysics: McGraw-Hill Book Co.

Keating, P. B., 1987, The inversion of time-domain electromagnetic data using the plate model: Ph.D. thesis, McGill Univ.

Keller, G. V., and Frischknecht, F. C., 1966, Electrical methods in geophysical prospecting: Pergamon Press.

Reed, L. E., 1981, The airborne electromagnetic discovery of the Detour zinc-copper-silver deposit, northwestern Quebec: Geophysics, **46,** 1278–1290.

Spector, A., and Bhattacharyya, B. K., 1966, Energy density spectrum and autocorrelation function of anomalies due to simple magnetic models: Geophys. Prosp., **14,** 242–272.

Spector, A., and Grant, F. S., 1970, Statistical models for interpreting aeromagnetic data: Geophysics, **35,** 293–302.

Telford, W. M., Geldart, L. P., Sheriff, R. E., and Keys, D. A., 1976, Applied geophysics: Cambridge Univ. Press.

Thomson, S., 1987, A new transient airborne EM system—GEOTEM: Presented at the 3rd Decennial Intl. Conf. on Geophys. and Geochem. Explor. for Minerals and Groundwater, Toronto, Ont.

Wesley, J. P., 1958, Response of dyke to oscillating dipole: Geophysics, **23,** 128–133.

Zollinger, R. D., Morrison, H. F., Lazenby, P. G., and Becker, A., 1987, Airborne electromagnetic bathymetry: Geophysics, **52,** 1127–1137.